

Observation of Coherent Oscillations in a Single Electron Spin

F. Jelezko, T. Gaebel, I. Popa, A. Gruber, and J. Wrachtrup

3. Physikalisches Institut, Universität Stuttgart, Stuttgart, Germany

(Received 2 September 2003; published 20 February 2004)

Rabi nutations and Hahn echo modulation of a single electron spin in a single defect center have been observed. The coherent evolution of the spin quantum state is followed via optical detection of the spin state. Coherence times up to several microseconds at room temperature have been measured. Optical excitation of the spin states leads to decoherence. Quantum beats between electron spin transitions in a single spin Hahn echo experiment are observed. A closer analysis reveals that beats also result from the hyperfine coupling of the electron spin to a single ^{14}N nuclear spin. The results are analyzed in terms of a density matrix approach of an electron spin interacting with two oscillating fields.

DOI: 10.1103/PhysRevLett.92.076401

PACS numbers: 71.55.-i, 03.65.Yz, 03.67.Pp, 76.30.Mi

Detection and manipulation of single electron spin states in solids have recently received much attention in the context of quantum computing [1–4]. Mainly, this is because localized electron spins in solids show long relaxation [5] and coherence times and their states can be easily manipulated via microwave or radio frequency pulses. Yet reading out a single spin state, a prerequisite for most quantum algorithms, has remained a major challenge up to now. Although single spin detection has been reported previously [6,7], most of the systems and techniques have not shown the ability to measure the quantum state of a single electron spin. The only solid state system where this has been successful is the nitrogen-vacancy (NV) defect center in diamond. The defect consists of a substitutional ^{14}N atom and a vacancy in an adjacent site and is known to have a strongly dipole allowed optical transition between its electron spin triplet ground state (3A) and a first excited spin triplet state (3E) (Fig. 1) [8]. Fluorescence emission strongly depends on the electron spin quantum state, which has led to optically detected magnetic resonance on single defect centers [9]. Electron spin relaxation times (T_1) of defect centers in diamond range from milliseconds at room temperature [10] to seconds at low temperature. Recently, electron spin quantum jumps have been detected [11], thus showing that the *spin state of a single electron spin* could be determined in this defect center. In this Letter we report on the generation of coherence among single electron spin states in the NV center. We analyze how spin coherence is influenced by optical excitation and coupling to additional degrees of freedom, like single ^{14}N nuclear spins of the NV center.

Single spin coherence in solids has been observed before [12,13]. However, the NV center in diamond is particularly interesting because of its electron paramagnetic ground state. Contrary to other systems, like organic molecules, the spin coherence time is thus not limited by the electronic lifetime of the state. Above all, the electron spin state can be read out directly via optical excitation and subsequent fluorescence relaxation. Pre-

viously this has been the basis of a number of ingenious studies on NV center ensembles, like the observation of electromagnetic induced transparency [14] and dressed state nutation [15].

Experiments have been carried out with a home-built confocal microscope operating in a temperature range between 2 and 300 K. Microwaves (MW) are coupled to the sample by a miniaturized short cut loop connected to a 40 W traveling wave tube amplifier to generate microwave H fields large enough for short microwave pulses. As sample material, 20 nm sized nanocrystallites made of high-pressure, high-temperature diamond (type 1b) have been used. Nanocrystals are preferred over bulk single crystal diamond, since the losses of fluorescence light due to the total internal reflection on a bulk diamond surface are avoided. To allow for comparison with a density matrix based theory, all experiments have been time averaged over 10^5 to 10^7 cycles to obtain smooth

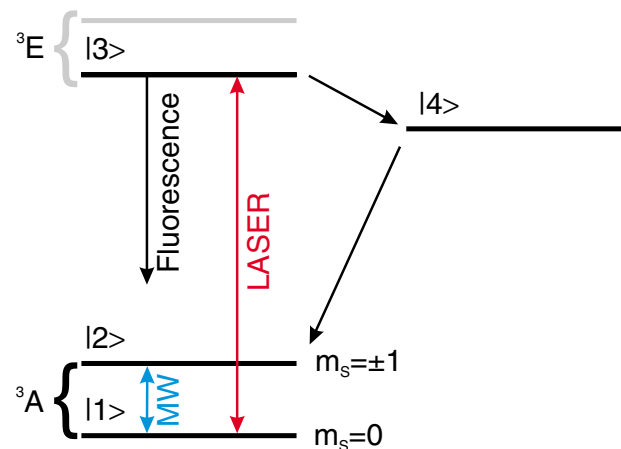


FIG. 1 (color online). Energy level scheme of the nitrogen vacancy defect center in diamond. The excited state spin manifold can be approximated by a single spin sublevel, since nonresonant optical excitation has been used in the experiment (see text). The greyed out lines correspond to the $m_s = \pm 1$ sublevels.

curves. To investigate the effect of optical excitation on the coherence properties of the electron spin transition, the defect was subjected to continuous laser irradiation ($\lambda = 514$ nm) in the first part of the experiments.

The ground and excited electron states of the NV defect are spin triplets ($S = 1$) with spin sublevels $m_s = 0, \pm 1$ (Fig. 1) [16]. The degeneracy among the sublevels is lifted due to either the mutual dipolar interaction of the two unpaired electron spins or an external magnetic field. Most of the experiments in this paper have been performed without applying an external magnetic field. Because of the C_{3v} symmetry of the defect, the $m_s = \pm 1$ sublevels remain degenerated ($E = 0$) but are split from the $m_s = 0$ sublevel by roughly 2.9 GHz. Fluorescence of a single defect center is visible only when the spin is in the $m_s = 0$ spin sublevel. Optical excitation leads to a strong spin polarization, such that, averaged in time, the electron spin is found with at least 70% probability in the $m_s = 0$ sublevel. The application of a resonant microwave pulse causes a transition of the system between the spin levels and thus modulates the fluorescence intensity. When time averaged, the nutation of the electron spin due to coherent interaction of the spin with the microwave H field is described as $r_3(t) = r_3(0)(1/\varpi^2)(\Delta\omega^2 + \omega_1^2 \cos\varpi t)$, where $\Delta\omega$ is the detuning between microwave and transition frequency and $\varpi = \sqrt{\Delta\omega^2 + \omega_1^2}$, with ω_1 the microwave Rabi frequency [17]. $r_3(t)$ is the difference between the probability to find the system in the $m_s = 0$ and $m_s = \pm 1$ sublevel. Figure 2 shows the nutation of a single NV center electron spin. Since coupling to the microwave and optical field has to be considered, the

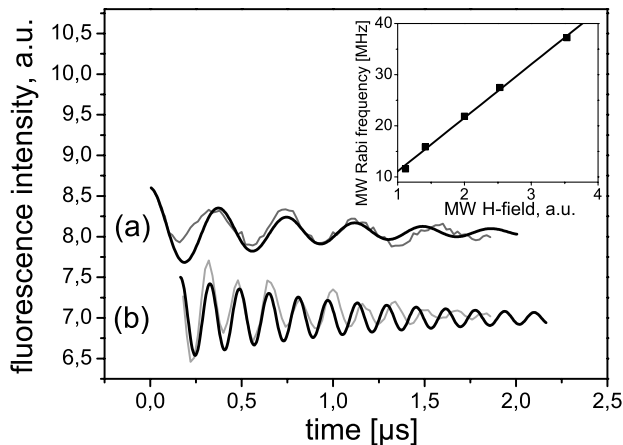


FIG. 2. Optically detected Rabi oscillations of single electron spins in a single NV defect center are shown for two values of the MW Rabi frequency; curve (a) corresponds to a slow MW Rabi frequency (approximately 16 MHz), and curve (b) corresponds to a faster Rabi frequency (39 MHz). The solid grey lines represent the measured data, and the thick lines show the simulations based on the microwave optical Bloch equations described in the text. The inset shows the dependence of the observed modulation frequency on the magnetic field of the applied microwave.

above mentioned equation has to be extended and experiments are compared with microwave-optical Bloch equations starting from the semiclassical Hamiltonian

$$\mathcal{H} = \sum_i \hbar\omega_i |i\rangle\langle i| - \hbar\Omega \cos(\omega_L t) (|1\rangle\langle 3| + |3\rangle\langle 1|) - \hbar\Lambda \cos(\omega_M t) (|1\rangle\langle 2| + |2\rangle\langle 1|).$$

In this equation $\hbar\omega_i$ is the energy of the ground and the excited states, $\Omega = E_0 d_{13}/\hbar$ is the Rabi frequency corresponding to the amplitude of the laser electric field E_0 , at frequency $\nu_L = \omega_L/2\pi$, interacting with the defect center transition dipole moment d_{13} . $\Lambda = \gamma H$ is the Rabi frequency of the ESR transition between the $m_s = 0$ and ± 1 states with frequency $\nu_M = \omega_M/2\pi$. The interaction between the molecule and the applied field is described by the Liouville equation for the electronic density matrix ρ , $i\hbar\dot{\rho} = [\mathcal{H}, \rho]$, in which all the populations are considered. However, all coherences, nonresonant with an external field, may be neglected. Coupling to phonons and surrounding spins appears in the reduced Liouville equation as dephasing and relaxation rate constants. The decay measured in the nutation experiment is determined by the electron spin dephasing time T_2 . Under low optical excitation, decay times range from 1.5 to 2 μ s, depending on the defect center under study. Recently, ensemble experiments have shown that T_2 in this system can reach values larger than 30 μ s [18], with increasing T_2 in samples with low nitrogen content. Our samples were not optimized for low nitrogen concentration, which explains the relatively short T_2 times in the present experiments. The most important source for dephasing in this system occurs via spin flip-flop processes between the electron spin of the NV center and the electron spins of the residual nitrogen impurities in the diamond lattices (P_1 , $S = 1/2$, single substitutional ^{14}N atom). For this case, the dephasing rate is strongly distance dependent ($1/r^3$). We found a substantial difference among the T_2 values of different NV centers, possibly due to a change in the distance between the electron spin of the center and the next nearest neighbor nitrogen in the lattice.

In the experiment, we observed a decrease in the decay time of the spin nutation upon increased optical excitation intensity. Figure 3 shows experimental data together with theoretically predicted curves. Since the laser excitation is nonresonant with the $^3A-^3E$ transition, fast (ps) internal conversion processes will effectively result in a noncoherent optical excitation. Under nonsaturating conditions one expects a linear dependence of the spin dephasing rate, as found in the experiment. It should be noted that in the microwave-optical Bloch equations, the differential equation for the coherence between the spin sublevels ρ_{12} (or ρ_{21}) does not directly comprise optical pumping. Rather the effect of optical pumping enters via ρ_{11} , which is a function of the optical excitation frequency. As a consequence in the experiment (data not shown) the time constant for fluorescence recovery after a

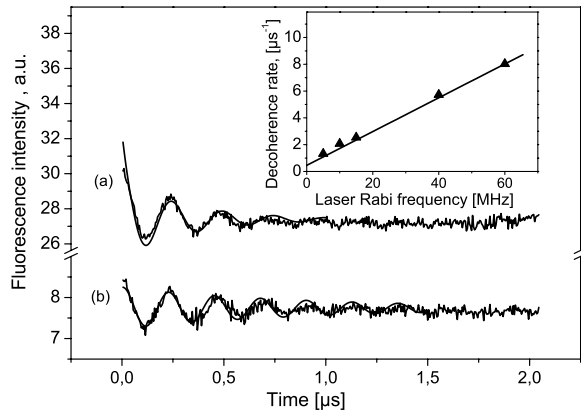


FIG. 3. Damping of spin coherence as a function of optical Rabi frequency. The defect center was subjected to continuous optical excitation in these experiments. The MW power was held constant, while the laser power was gradually increased. Curves (a) and (b) represent the nutation curves for two different values of the laser power (corresponding laser Rabi frequencies were 40 and 7 MHz, respectively). The experimental data are shown in grey, and the theoretical curves in thick lines. The inset shows the nutation damping time versus optical Rabi frequency. The symbols show the experimental data. The curve was calculated according to the model presented in the text. The nutation damping time is decreasing upon increasing the optical excitation power.

microwave pulse (T_1) shows the same dependence on optical pumping as the coherence (T_2). Assuming a single spin experiment that is not time averaged, our finding is explained similar to results from previously reported experiments on single ions [19]. There, optical excitation and emission have been related to a measurement process on the spin state. This leads to a projection of the spin state in one of its eigenstates. Consequently, an increase in the excitation frequency is followed by a decrease in the damping time of spin coherence. An important prerequisite for probing unperturbed electron spin coherence is thus to carry out spin manipulation in the absence of optical excitation. In this scheme, state preparation results from optical excitation, i.e., the spin is brought to the $m_s = 0$ state via optical pumping. Subsequently, the laser is switched off and microwave pulses are applied and the final result is measured via laser excitation and fluorescence emission. The experiments described below follow this scheme.

In order to probe how well the single spin state can be coherently manipulated by microwave pulses, the spin state evolution under a Hahn echo pulse sequence has been investigated. Adapted to optically detected magnetic resonance, the Hahn echo pulse sequence consists of the well-known 90° - τ - 180° - τ' microwave pulses and waiting times followed by a 90° pulse to convert the spin echo phenomenon into populations, measurable by fluorescence detection [20]. Figure 4 shows the single spin Hahn echo together with echo decay measurements. The Hahn echo sequence refocuses inhomogeneously distrib-

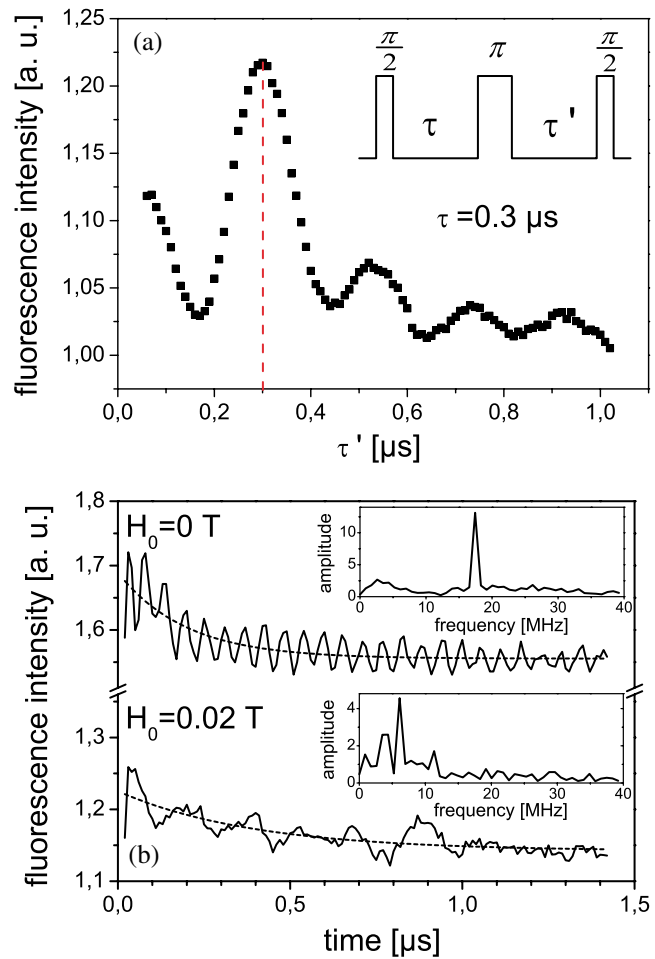


FIG. 4 (color online). (a) Hahn echo of a single NV center electron spin in low magnetic field (0.006 T). The applied MW sequence is depicted together with the experimental data. The Hahn echo occurs for a value of the delay time $\tau = \tau' = 0.3 \mu\text{s}$. (b) Hahn echo decay curve of a single electron spin at zero external field and in a field $H_0 = 0.02 \text{ T}$. The inset shows the Fourier transform of the respective echo decays after subtraction of the exponential decay term (dashed line).

uted ESR transition frequencies, if this distribution is static on the time scale of the echo sequence. Indeed, when time averaged, we found an inhomogeneously broadened ESR resonance line. The source of the inhomogeneity becomes apparent when the Hahn echo amplitude is followed as a function of the waiting time $\tau = \tau'$. Superimposed on the echo decay, which marks T_2 , a strong modulation shows up. This echo envelope modulation is a well-known phenomenon from bulk ESR measurements [21]. It results from a beating between different transitions within the ESR resonance spectrum, all excited coherently by the microwave pulse. A Fourier transform of the echo decay function after subtracting the exponential decay itself reveals a characteristic frequency of 17 MHz. This corresponds well with the measured splitting between the $m_s = +1$ and -1 state of the particular defect studied. This splitting is the result of a slight deviation from C_{3v} symmetry of the defect. Since the

microwave Rabi frequency ω_1 is substantially larger than the frequency splitting $\Delta\omega$ between the two states, both transitions are excited simultaneously. To confirm our interpretation a small external magnetic field H_0 was applied. The Hamiltonian which now describes the system is $\mathcal{H} = SDS + g_e\beta_eSH_0 + SAI - g_n\beta_nIH_0$, where D and A are the fine structure and hyperfine splitting tensors, and $g_{e,n}$ and $\beta_{e,n}$ are the electron and nuclear g factors and Bohr magnetons, respectively. The electron Zeeman term further splits the $m_s = \pm 1$ levels. For an H_0 field of 0.02 T, the splitting is roughly 150 MHz, such that the microwave pulse excites only the $m_s = 0$ to -1 transition. As a result the beating in the Hahn echo due to the interference between the two electronic transitions disappears. Instead, a modulation with much lower frequency appears. The Fourier transform now shows frequency components between 5 and 10 MHz. Following a previous analysis of Hahn echo decay data on NV center ensembles [22], we believe that this envelope modulation arises from hyperfine coupling of the electron spin to ^{14}N nuclear spins of the NV centers. Because of the low spin density of the electrons at the location of the nucleus, the hyperfine coupling of ^{14}N usually is not resolved in the ESR spectrum [23]. Although the frequency components caused by this ^{14}N are also visible in the echo decay data for $H_0 = 0$ T, they are considerably more pronounced when a small magnetic field is applied. In order to detect the nuclear modulation effect allowed ($\Delta m_I = 0$) as well as forbidden ($\Delta m_I = \pm 1$), ESR transitions have to be excited. The modulation depth is largest when the nuclear Zeeman splitting ω_I equals the hyperfine frequency, i.e., $\omega_I = |m_s|A_{\text{iso}}$, where A_{iso} is the isotropic hyperfine coupling. Under this condition, the nuclear spin is no longer quantized along the external magnetic field. The allowed and forbidden ESR transitions have the same magnitude, and the modulation depth is at maximum [21]. This condition is met for the experiment shown [Fig. 4(b)] where $H_0 = 0.02$ T. Hyperfine coupling to ^{14}N also explains the beating seen in Fig. 4(a). If ω_M is detuned by $\Delta\omega$ from the spin resonance transition, the echo is expected to be modulated by $\cos[\Delta\omega(\tau - \tau')]$, where $\Delta\omega$ is the hyperfine coupling. Indeed, the observed modulation frequencies correspond well with those found in the Fourier transform of the Hahn echo decay in an external magnetic field.

In summary, we report on the first experimental investigation of coherent oscillations among spin sublevels of a ground state single electron spin at room temperature. The measured dephasing times range from 1 to 2 μs . They strongly depend on the optical excitation frequency, which is in good agreement with microwave-optical Bloch equations. The coherence times are long enough to allow for a coherent manipulation of the single spin. These experiments reveal the hyperfine interaction of the electron with the ^{14}N nuclear spin of the defect center. Since our experiments demonstrate a coherent evolution of electron spin transitions for different nitrogen nuclear

spin configurations, they may be a first step towards conditional nontrivial two single spin quantum logical operations.

This work was supported by DFG under the framework of project ‘‘Quanten-Informationsverarbeitung,’’ Landesstiftung BW, and EU Project No. IST-2001-37150 QIPDDF-ROSES. One of the authors (I.P.) acknowledges the support of the Graduiertenkolleg Magnetische Resonanz Universitat Stuttgart.

-
- [1] B. E. Kane, *Nature (London)* **393**, 133 (1998).
 - [2] R. G. Clark *et al.*, *Philos. Trans. R. Soc. London A* **361**, 1451 (2003).
 - [3] A. M. Stoneham, A. J. Fisher, and P. T. Greenland, *J. Phys. Condens. Matter* **15**, L447 (2003).
 - [4] *Semiconductor Spintronics and Quantum Computation*, edited by D. D. Awschalom, D. Loss, and N. Samarth (Springer-Verlag, Berlin, 2002).
 - [5] G. Feher, *Phys. Rev.* **114**, 1219 (1959).
 - [6] J. Kohler, J. A. J. M. Disselhorst, M. C. J. M. Donckers, E. J. J. Groenen, J. Schmidt, and W. E. Moerner, *Nature (London)* **363**, 242 (1993).
 - [7] J. Wrachtrup, C. von Borczyskowski, J. Bernard, M. Orrit, and R. Brown, *Nature (London)* **363**, 244 (1993).
 - [8] *Properties and Growth of Diamond*, edited by G. Davies (INSPEC, London, 1994).
 - [9] A. Gruber, A. Drabenstedt, C. Tietz, L. Fleury, J. Wrachtrup, and C. von Borczyskowski, *Science* **276**, 2012 (1997).
 - [10] E. C. Reynhardt and G. L. High, *J. Chem. Phys.* **109**, 4090 (1998).
 - [11] F. Jelezko, I. Popa, A. Gruber, and J. Wrachtrup, *Appl. Phys. Lett.* **81**, 2160 (2002).
 - [12] J. Wrachtrup, C. von Borczyskowski, J. Bernard, M. Orrit, and R. Brown, *Phys. Rev. Lett.* **71**, 3565 (1993).
 - [13] A. C. J. Brouwer, E. J. J. Groenen, and J. Schmidt, *Phys. Rev. Lett.* **80**, 3944 (1998).
 - [14] E. A. Wilson, N. B. Manson, and C. Wei, *Phys. Rev. A* **67**, 023812 (2003).
 - [15] C. Wei, N. B. Manson, and J. P. D. Martin, *Phys. Rev. Lett.* **74**, 1083 (1995).
 - [16] D. A. Redman, S. Brown, R. H. Sands, and S. C. Rand, *Phys. Rev. Lett.* **67**, 3420 (1991).
 - [17] W. G. Breiland, H. C. Brenner, and C. B. Harris, *J. Chem. Phys.* **62**, 3458 (1975).
 - [18] T. A. Kennedy, F. T. Charnock, J. S. Colton, J. E. Butler, R. C. Linares, and P. J. Doering, *Phys. Status Solidi (b)* **233**, 416 (2002).
 - [19] W. M. Itano, J. J. Bollinger, and D. J. Wineland, *Phys. Rev. A* **41**, 2295 (1989).
 - [20] W. G. Breiland, C. B. Harris, and A. Pines, *Phys. Rev. Lett.* **30**, 158 (1973).
 - [21] W. B. Mims, *Phys. Rev. B* **5**, 2409 (1972).
 - [22] F. T. Charnock and T. A. Kennedy, *Phys. Rev. B* **64**, 041201 (2001).
 - [23] X.-F. He, N. B. Manson, and P. T. H. Fisk, *Phys. Rev. B* **47**, 8816 (1992).